

Autothermotaxis of volatile drops

Pallav Kant ^{1,2,*} Mathieu Souzy ^{1,3,†} Nayoung Kim ^{1,‡}
Devaraj van der Meer ^{1,§} and Detlef Lohse ^{1,4,¶}

¹*Physics of Fluids Group, Max Planck Center Twente for Complex Fluid Dynamics, University of Twente, 7500 AE Enschede, The Netherlands*

²*Bullard Laboratories, Department of Earth Science, University of Cambridge, CB3 0EZ United Kingdom*

³*INRAE, Aix Marseille Univ, UMR RECOVER, 3275 Rte de Cézanne, CS 40061, 13182 Aix-en-Provence, Cedex5, France*

⁴*Max Planck Institute for Dynamics and Self-Organization, Am Fassberg 17, 37077 Göttingen, Germany*



(Received 9 June 2023; accepted 15 November 2023; published 31 January 2024)

When a drop of a volatile liquid is deposited on a uniformly heated wettable, thermally conducting substrate, one expects to see it spread into a thin film and evaporate. Contrary to this intuition, due to thermal Marangoni contraction, the deposited drop contracts into a spherical-cap-shaped puddle, with a finite apparent contact angle. Strikingly, this contracted droplet, above a threshold temperature, well below the boiling point of the liquid, starts to spontaneously move on the substrate in an apparently erratic way. We describe and quantify this self-propulsion of the volatile drop. It arises due to spontaneous symmetry breaking of thermal Marangoni convection, which is induced by the nonuniform evaporation of the droplet. Using infrared imaging, we reveal the characteristic interfacial flow patterns associated with Marangoni convection in the evaporating drop. A scaling relation describes the correlation between the moving velocity of the drop and the apparent contact angle, both of which increase with the substrate temperature.

DOI: [10.1103/PhysRevFluids.9.L012001](https://doi.org/10.1103/PhysRevFluids.9.L012001)

Inkjet printing [1–5], spray cooling [6,7], self-assembly techniques [8–12], and forensic science [13,14] all rely on controlled evaporation of a droplet on a surface. In their seminal work, Deegan *et al.* [15–17] have shown that nonuniform evaporation of a droplet deposited on a surface establishes a capillary flow that continuously compensates for enhanced evaporative losses at the edge of the droplet. The corresponding flow field, however, can be affected by interfacial (Marangoni) flow induced by a gradient in temperature along the interface, also due to the nonuniform evaporation [1,18–20]. Interestingly, the direction of thermal gradient and the consequent Marangoni flow is critically influenced by the heat exchange between the droplet and the substrate [21].

In this letter, we demonstrate that spontaneous symmetry breaking of this Marangoni flow can lead to self-propulsion of a volatile droplet on a warm, thermally conducting substrate. Note that,

*kantpallav88@gmail.com

†mathieu.souzy@inrae.fr

‡nayoungkim516@gmail.com

§d.vandermeer@utwente.nl

¶d.lohse@utwente.nl

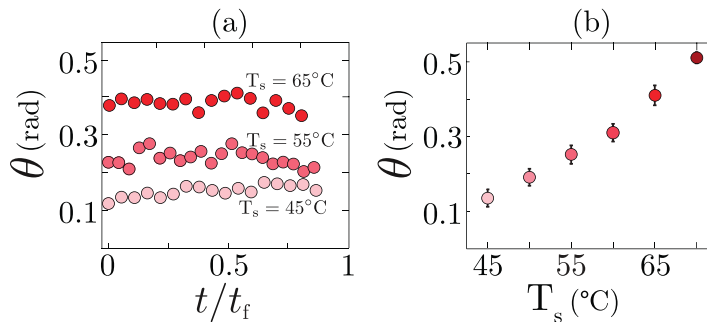


FIG. 1. (a) Temporal measurement of apparent contact angle θ during the lifetime of the droplet for different substrate temperature T_s . Time is nondimensionalized using the droplet lifetime t_f . (b) Increase in the contact angle θ of a self-propelling ethanol droplet with T_s .

unlike the motion of a droplet in the presence of a thermal [22–24], chemical [25–27], electrical [28], or photochemical [29] extrinsic gradient, the impetus for the self-propulsion observed in our system originates from the inherently unstable internal thermal Marangoni convection. This intrinsic self-propulsion characteristic distinguishes this phenomenon from the previously reported freely moving volatile droplets on immiscible aqueous baths [30–32], where the cause of the motion is external to the droplet. However, parallels can be drawn between our system and the self-propulsion of dissolving droplets (autochemotaxis), which generate propulsion forces due to intrinsically unstable solutal Marangoni flows in an isotropic surrounding medium [33–38]. Therefore, we call the phenomenon *autothermotaxis*.

Deposition of a small volume of pure ethanol ($\sim 4 \mu\text{L}$) on a horizontal sapphire plate at room temperature yields a thin film with a vanishing contact angle $\theta \sim 0^\circ$, which evaporates slowly over time. This behavior is expected for a substrate-liquid pair for which the spreading parameter $S = \gamma_{sv} - (\gamma_{sl} + \gamma_{lv})$ is positive; here, γ_{ij} denotes the interfacial tension between i - j phases, namely, substrate (s), liquid (l), and vapor (v). However, despite the favorable wetting conditions, when the same volume of ethanol is deposited on a uniformly heated sapphire plate, it contracts into a spherical-cap-shaped droplet, exhibiting a finite apparent contact angle. For a droplet deposited on a substrate such that their thermal conductivity ratio $k_R = k_{\text{sub}}/k_{\text{drop}} \gg 2$ (here, for ethanol on sapphire, $k_R = 228$), this contraction is caused by the evaporation-induced thermal Marangoni flow that is directed radially inwards along the droplet interface [21,39,40]. The resulting apparent droplet contact angle after the thermal Marangoni contraction is shown in Fig. 1; for fixed surface temperature, it is roughly constant in time but becomes larger with increasing surface temperature, reflecting the stronger thermal Marangoni flow.

We now come to the main finding of this letter, namely, beyond a threshold temperature $T_{\text{onset}} \sim 45^\circ\text{C}$, the Marangoni contracted ethanol droplets spontaneously start to move in a seemingly erratic fashion along the substrate. This self-propulsion of an ethanol droplet persists until it has evaporated entirely at time $t = t_f$; see Fig. 2 and the movies in the Supplemental Material [41]. We emphasize that the self-propulsion of a volatile droplet as reported here occurs at temperatures much lower than its boiling point T_b , which for ethanol is $T_b = 78^\circ\text{C}$. Therefore, it bears no commonality with mobile Leidenfrost droplets on strongly superheated surfaces [42–44]. Additionally, the observed self-propulsion of droplets is not exclusive to the ethanol-sapphire combination; it is also evident in various combinations of volatile liquids and substrates; see Table I. However, to keep the discussion concise, we focus on the fundamental characteristics of this phenomenon using the ethanol-sapphire system.

Overlaid images in Fig. 2 illustrate the contrasting behaviors of a self-propelling ethanol droplet at two different substrate temperatures. At lower temperatures, the self-propelling droplet moves slowly and uniformly [Fig. 2(a)], whereas fast and chaotic movements are observed at higher

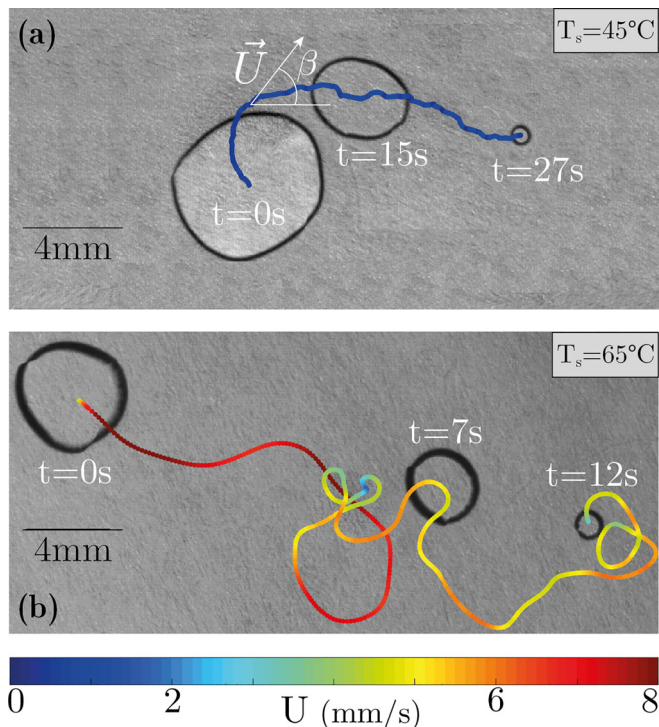


FIG. 2. Chronophotography of volatile ethanol droplets of volume $4\ \mu\text{L}$, deposited on a horizontal heated sapphire plate at temperature (a) $T_s = 45\ ^\circ\text{C}$ and (b) $T_s = 60\ ^\circ\text{C}$. Following a short transient period after deposition, the droplet self-propels (autothermotaxis) until complete evaporation. Trajectories are overlaid on the images and color-coded by instantaneous velocity U . Droplets move faster and have an increased tendency to reorient on warmer substrates.

temperatures [Fig. 2(b)]. The distribution of propulsion velocities U measured at different substrate temperatures, shown in Fig. 3(a), demonstrates this systematic shift toward faster velocities with increasing substrate temperature. Note that, at elevated temperatures, the motion of a droplet is largely unaffected by surface heterogeneities (roughness), whereas self-propelling droplets at low substrate temperatures are more prone to pinning. Further, as highlighted in Fig. 3(b), on warmer substrates, the fast motion of a droplet is also coupled with an increased tendency for abrupt reorientations. This type of motion is reminiscent of a run-and-tumble movement observed in

TABLE I. Thermal conductivity ratio $k_R = k_{\text{sub}}/k_{\text{drop}}$ and threshold temperature T_{onset} for various liquid-substrate combinations, revealing the generic nature of autothermotaxis.

$k_R T_{\text{onset}}$	Novec 7100	IPA	Ethanol	Acetone
Boiling point	61°C	82.5°C	78°C	56°C
Aluminium	3464 < 20°C	1770 40°C	1398 40°C	1328 40°C
Sapphire	565 < 20°C	289 45°C	228 45°C	216 45°C
Glass	11.6 < 20°C	5.9 45°C	4.7 45°C	4.4 No Motion
Acrylic	2.9 No Motion	1.5 No Motion	1.2 No Motion	1.1 No Motion

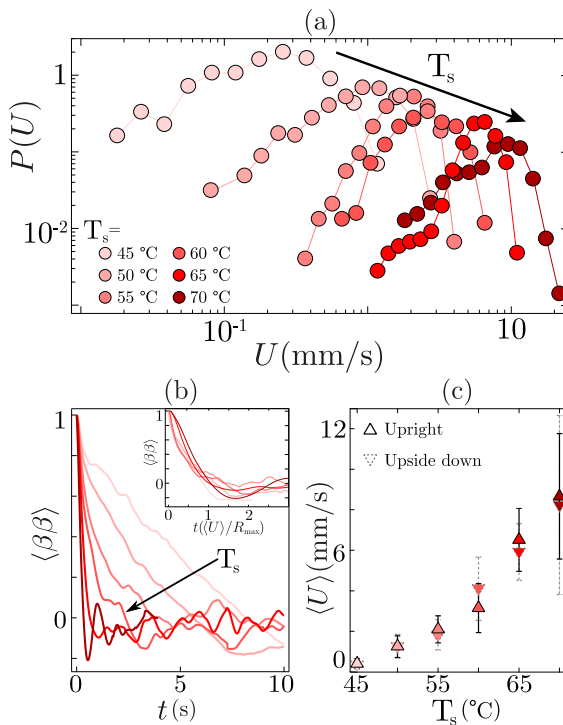


FIG. 3. (a) Probability distribution function of velocity $P(U)$ of ethanol droplets on a warm sapphire plate for different substrate temperatures T_s . (b) Autocorrelation function of the orientation angle β with increasing T_s . Inset: Data collapse when nondimensionalizing time with the maximum droplet radius R_{\max} and the mean velocity $\langle U \rangle$. (c) Comparison of the mean velocity $\langle U \rangle$ of the droplet measured in upright and upside-down configurations. Error bars represent the standard deviation of the velocities. Close match between the two configurations highlights the insignificant role of gravity in the droplet motion.

self-phoretic biological systems and artificial microswimmers [38,45,46]. We quantify the tendency of a moving droplet to reorient itself by measuring the autocorrelation function $\langle \beta \beta \rangle = \frac{\langle \beta(t'+t)\beta(t) \rangle_t}{\langle \beta(t') \rangle_t^2}$ of its orientation angle β ; see Fig. 2. As shown in Fig. 3(b), the quick decay of the autocorrelation function at higher temperatures demonstrates that faster-moving droplets lose their directionality more rapidly. As shown in the inset of Fig. 3(b), by nondimensionalizing time, using mean velocity $\langle U \rangle$ and maximum droplet radius R_{\max} , a collapse of $\langle \beta \beta \rangle$ indicates that, irrespective of the substrate temperature, a moving droplet reorients itself after moving typically about one radius. Importantly, since a reorientation event consists of a droplet slowing down while changing direction and then reaccelerating along a new path, the droplet velocity on warmer substrates varies dramatically over its lifetime. As a result, both the mean and standard deviation of the velocity of a droplet increase with temperature. A close comparison between the mean velocity $\langle U \rangle$ of moving droplets in upright and upside-down orientations [Fig. 3(c)] shows that effects arising from density changes due to temperature variations (i.e., thermal convection) within the droplet play no significant role in the overall dynamics, reflecting that the corresponding Archimedes number (the ratio between buoyancy forces due to temperature-induced density differences and viscous forces) [47] is < 1 , namely, $Ar = gh^3 \rho_{\text{warm}} (\rho_{\text{cold}} - \rho_{\text{warm}}) / \mu^2$, see the Supplemental Material [41].

The two main arising questions are: Why does the volatile droplet move spontaneously on the uniform surface, without any extrinsic asymmetry, and how (if at all) is this spontaneous motion of the evaporating droplet related to its thermal Marangoni contraction?

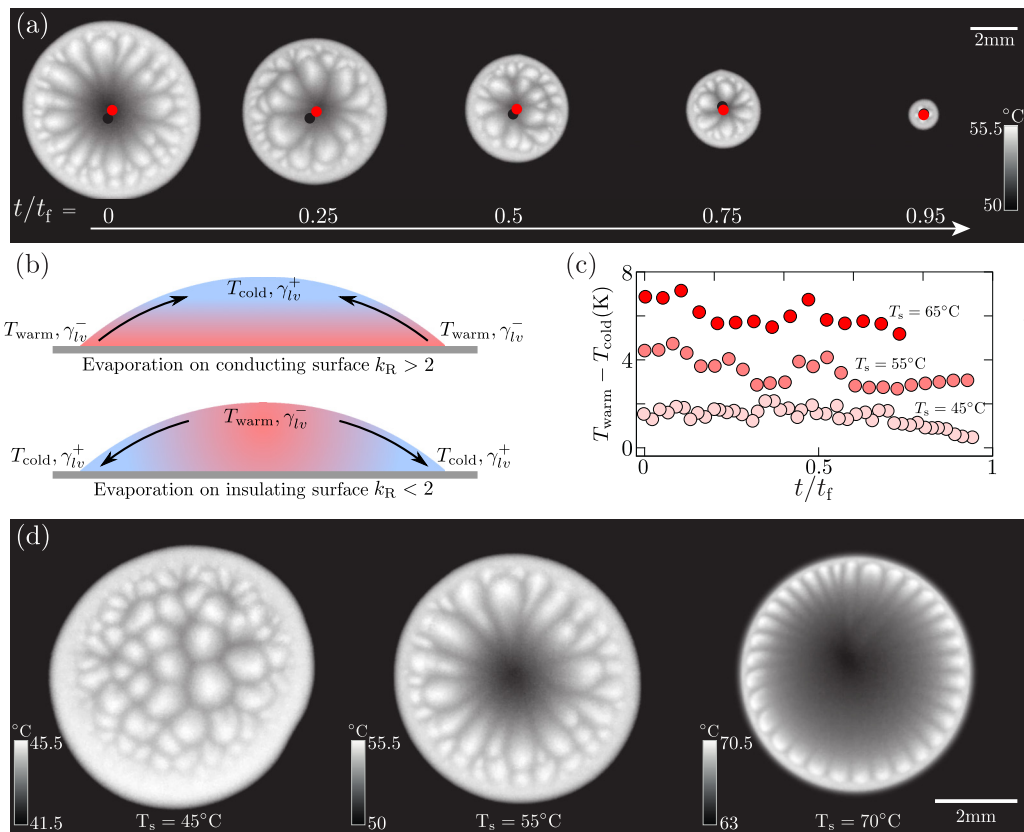


FIG. 4. Infrared imaging of self-propelling droplets: (a) Interfacial thermal map (top view) of a moving ethanol droplet while it evaporates on a sapphire substrate at $T_s = 55^\circ\text{C}$. The bright region close to the contact line is the warmest part of the droplet, whereas the dark region near the apex is the coldest. Red and blue dots corresponding, respectively, to the centroid of droplet footprint and convection cells reveal the spontaneous symmetry breaking of the Marangoni flow. (b) Sketches of the thermal gradient and the resulting Marangoni flows for an evaporating droplet on a heated conducting ($k_R > 2$) and on an insulating ($k_R < 2$) substrate. (c) Temperature difference between the warmest and coldest part of a self-propelling ethanol droplet for various T_s . (d) Variation in interfacial temperature patterns with substrate temperature $T_s = 45, 55,$ and 70°C .

To reveal the underlying physical mechanism, we make use of infrared (IR) imaging, allowing quantitative measurement of the interfacial thermal activity. Figure 4(a) shows the interfacial thermal map of a self-propelling ethanol droplet deposited on a sapphire plate at $T_s = 55^\circ\text{C}$ at different instances of its lifetime. As anticipated, for a droplet substrate pair with $k_R \gg 2$, the conduction between the substrate and the liquid suppresses the evaporative cooling effect near the contact line; thus, it is the warmest region (T_{warm}) on the interface. In contrast, the apex of the droplet is the coldest region (T_{cold}). Our measurements indicate that the difference in the temperature of these two regions on the droplet interface $\Delta T = T_{\text{warm}} - T_{\text{cold}}$ remains nearly constant throughout the lifetime of the droplet while increasing with a rise in the substrate temperature; see Fig. 4(c). Correspondingly, the persistent stronger Marangoni flow along the interface facilitates the enhanced contraction of a droplet on warmer substrates.

Strikingly, these IR images also reveal the presence of nonstationary convective patterns on the droplet interface; see also the movies in the Supplemental Material [41]. The emergence of such patterns is a signature of a flow instability of the evaporating droplet that is driven by

thermal Marangoni flow originating from the variations of surface tension with temperature [48–52]. Importantly, the resultant unsteady patterns are also indicative of an unsteady flow field inside the droplet, exhibiting spontaneous symmetry breaking. This spontaneous symmetry breaking of the flow field manifests itself through the asymmetric arrangement of convective cells. This is confirmed by comparing the centroid of the interfacial convection cells with the center of the droplet footprint, as shown in Fig. 4(a). The spontaneous symmetry breaking of the unsteady flow field provides the impetus for the self-propulsion of a droplet, like for the self-propulsion of a dissolving droplet by solutal Marangoni flow [33–38].

We emphasize that there is no causal relationship between the Marangoni contraction of droplets and the Marangoni instability of evaporating droplets. These two distinct mechanisms govern two different aspects of the thermal Marangoni flow, namely, contraction and lateral motion by spontaneous symmetry breaking.

The Marangoni instability in the evaporating ethanol droplet manifests itself through distinct convective patterns, depending on the substrate temperature. Figure 4(d) shows a comparison of distinct patterns exhibited by ethanol droplets at different substrate temperatures. At lower substrate temperatures, the convective pattern includes irregularly shaped convection cells distributed randomly over the droplet interface, which is also reminiscent of disordered Marangoni convection observed for a very thin liquid layer heated from the bottom [53]. In contrast, at higher temperatures, flowerlike patterns with azimuthally arranged convection cells appear. The aspect ratio and thus the apparent contact angle $\theta \sim h/R$, where h is the drop height and R its contact radius, determines the morphology of the convective pattern, as also demonstrated previously for heated liquid films in circular containers [54] or for Rayleigh-Bénard convection [55]. We also performed experiments with droplets with pinned contact lines to confirm the role of droplet aspect ratio in selecting convective patterns. In such a configuration, the droplet aspect ratio decreases steadily as the drop evaporates. Accordingly, this induces a striking transition of convective patterns; see the Supplemental Material [41].

Finally, we provide the correlation between the propulsion velocity and the apparent droplet contact angle. We obtain this by balancing the driving force of the droplet movement with the overall friction force, see Fig. 5(b): The Marangoni driving occurs after spontaneous symmetry breaking; thereafter, one Marangoni convection roll [or a few in three dimensions; see the bold blue roll in Fig. 5(b)] dominates the others, whose net forces on the droplet cancel out. As the aspect ratio of the convection rolls is roughly unity [55], the area A_M of the dominating Marangoni roll is determined by the Marangoni roll height h , i.e., $A_M \sim h^2$, and the resulting frictional Marangoni force on the droplet thus is $F_M \sim A_M U_M \mu / h$, with μ being the dynamic viscosity and $U_M \sim \frac{\Delta\sigma}{\mu} \sim \frac{1}{\mu} \frac{d\sigma}{dT} \Delta T$ being the Marangoni velocity. In contrast, the overall viscous friction force on the droplet with its overall velocity U acts on the whole droplet area $A_D \sim R^2$, i.e., $F_D \sim A_D \mu U / h$. The force balance $F_M \sim F_D$ thus results in $A_M U_M \sim A_D U$ or in the desired correlation:

$$\langle U \rangle \sim U \sim U_M \frac{h^2}{R^2} \sim \frac{1}{\mu} \frac{d\sigma}{dT} \Delta T \theta^2, \quad (1)$$

where we have assumed that $h/R = \tan \theta \approx \theta$ is small. Equation (1) thus indeed reflects the observed quadratic dependence of the average velocity $\langle U \rangle$ on the apparent contact angle θ of the Marangoni contracted droplet as observed in Fig. 5(a). Here, we have ignored the slight dependence of ΔT on the surface temperature [Fig. 4(c)]. Incorporating this dependence $\Delta T(T_s)$ slightly steepens the prediction but, within experimental error, remains consistent with our data, see the Supplemental Material [41]. Equation (1) also explains the observed steep increase of the average velocity $\langle U \rangle$ above the threshold temperature [Fig. 3(c)], as both ΔT [Fig. 4(c)] and θ (Fig. 1) increase with the surface temperature T_s . Additionally, it is important to highlight that the value of θ is contingent on the strength of the thermal gradient across the droplet interface which, in turn, is dictated by the ratio of thermal conductivities between the liquid and the substrate. This relationship is not straightforward, requiring further investigations in this direction.

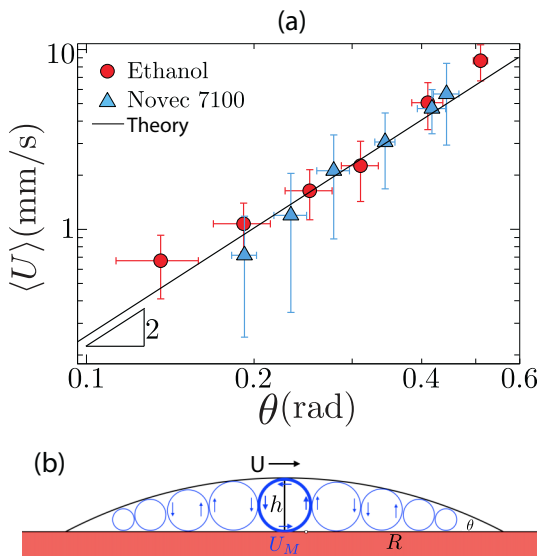


FIG. 5. (a) Mean droplet velocity $\langle U \rangle$ measured as a function of the apparent contact angle θ for ethanol and Novec 7100 droplets deposited on a warm sapphire plate. The solid black line is the expected scaling $\langle U \rangle \sim \theta^2$, cf. Eq. (1). Error bars represent the standard deviation over multiple runs. (b) Sketch of the Marangoni rolls inside the moving drop, after spontaneous symmetry breaking. See main text for explanations.

In summary, our experiments reveal a surprising phenomenon of self-propulsion that includes a volatile droplet and a uniformly heated wettable, conducting surface. Using IR imaging, we demonstrate that the spontaneous contraction of droplets coupled with spontaneous symmetry breaking of the Marangoni flow inside the droplet results in self-propulsion. Though results are mainly discussed in the context of ethanol on a sapphire substrate, we found that the self-propulsion is also observed for a variety of droplet-substrate pairs. These findings (exemplified in Table I) also verify the condition $k_R \geq 4.7$ for the occurrence of the investigated phenomenon and highlight its generic and robust nature, which can be a major hindrance for precise droplet deposition required for many applications such as inkjet printing. The next step, therefore, must be a detailed parameter study of the autothermotaxis of volatile droplets.

We thank S. Hardt, O. Shishkina, and J. Zhang for fruitful discussion on the subject. NWO is kindly acknowledged for financial support.

P.K., M.S., and N.K. contributed equally to this letter.

-
- [1] D. Lohse, Fundamental fluid dynamics challenges in inkjet printing, *Annu. Rev. Fluid Mech.* **54**, 349 (2022).
 - [2] P. Calvert, Inkjet printing for materials and devices, *Chem. Mater.* **13**, 3299 (2001).
 - [3] T. Shimoda, K. Morii, S. Seki, and H. Kiguchi, Inkjet printing of light-emitting polymer displays, *MRS Bull.* **28**, 821 (2003).
 - [4] J. Park and J. Moon, Control of colloidal particle deposit patterns within picoliter droplets ejected by ink-jet printing, *Langmuir* **22**, 3506 (2006).
 - [5] B. Derby, Inkjet printing of functional and structural materials: Fluid property requirements, feature stability, and resolution, *Annu. Rev. Mater. Res.* **40**, 395 (2010).

- [6] W. M. Grissom and F. Wierum, Liquid spray cooling of a heated surface, *Int. J. Heat Mass Transf.* **24**, 261 (1981).
- [7] J. Kim, Spray cooling heat transfer: The state of the art, *Int. J. Heat Fluid Flow* **28**, 753 (2007).
- [8] P. Jiang, J. Bertone, K. S. Hwang, and V. Colvin, Single-crystal colloidal multilayers of controlled thickness, *Chem. Mater.* **11**, 2132 (1999).
- [9] E. Rabani, D. R. Reichman, P. L. Geissler, and L. E. Brus, Drying-mediated self-assembly of nanoparticles, *Nature (London)* **426**, 271 (2003).
- [10] S. Narayanan, J. Wang, and X.-M. Lin, Dynamical self-assembly of nanocrystal superlattices during colloidal droplet evaporation by *in situ* small angle x-ray scattering, *Phys. Rev. Lett.* **93**, 135503 (2004).
- [11] M. Schnell-Levin, E. Lauga, and M. P. Brenner, Self-assembly of spherical particles on an evaporating sessile droplet, *Langmuir* **22**, 4547 (2006).
- [12] Á. G. Marín, H. Gelderblom, A. Susarrey-Arce, A. van Houselt, L. Lefferts, J. G. Gardeniers, D. Lohse, and J. H. Snoeijer, Building microscopic soccer balls with evaporating colloidal fakir drops, *Proc. Natl. Acad. Sci. USA* **109**, 16455 (2012).
- [13] F. Smith, C. Nicloux, and D. Brutin, A new forensic tool to date human blood pools, *Sci. Rep.* **10**, 1 (2020).
- [14] D. Attinger, C. Moore, A. Donaldson, A. Jafari, and H. A. Stone, Fluid dynamics topics in bloodstain pattern analysis: Comparative review and research opportunities, *Forensic Sci. Int.* **231**, 375 (2013).
- [15] R. D. Deegan, O. Bakajin, T. F. Dupont, G. Huber, S. R. Nagel, and T. A. Witten, Capillary flow as the cause of ring stains from dried liquid drops, *Nature (London)* **389**, 827 (1997).
- [16] R. D. Deegan, O. Bakajin, T. F. Dupont, G. Huber, S. R. Nagel, and T. A. Witten, Contact line deposits in an evaporating drop, *Phys. Rev. E* **62**, 756 (2000).
- [17] R. D. Deegan, Pattern formation in drying drops, *Phys. Rev. E* **61**, 475 (2000).
- [18] D. Lohse and X. Zhang, Physicochemical hydrodynamics of droplets out of equilibrium, *Nat. Rev. Phys.* **2**, 426 (2020).
- [19] Z. Wang, D. Orejon, Y. Takata, and K. Sefiane, Wetting and evaporation of multicomponent droplets, *Phys. Rep.* **960**, 1 (2022).
- [20] H. Gelderblom, C. Diddens, and A. Marin, Evaporation-driven liquid flow in sessile droplets, *Soft Matter* **18**, 8535 (2022).
- [21] W. Ristenpart, P. Kim, C. Domingues, J. Wan, and H. A. Stone, Influence of substrate conductivity on circulation reversal in evaporating drops, *Phys. Rev. Lett.* **99**, 234502 (2007).
- [22] F. Brochard, Motions of droplets on solid surfaces induced by chemical or thermal gradients, *Langmuir* **5**, 432 (1989).
- [23] J. Brzoska, F. Brochard-Wyart, and F. Rondelez, Motions of droplets on hydrophobic model surfaces induced by thermal gradients, *Langmuir* **9**, 2220 (1993).
- [24] A. L. Yarin, W. Liu, and D. H. Reneker, Motion of droplets along thin fibers with temperature gradient, *J. Appl. Phys.* **91**, 4751 (2002).
- [25] M. K. Chaudhury and G. M. Whitesides, How to make water run uphill, *Science* **256**, 1539 (1992).
- [26] F. D. Dos Santos and T. Ondarçuhu, Free-running droplets, *Phys. Rev. Lett.* **75**, 2972 (1995).
- [27] S. Daniel, M. K. Chaudhury, and J. C. Chen, Fast drop movements resulting from the phase change on a gradient surface, *Science* **291**, 633 (2001).
- [28] M. Gunji and M. Washizu, Self-propulsion of a water droplet in an electric field, *J. Phys. D* **38**, 2417 (2005).
- [29] K. Ichimura, S.-K. Oh, and M. Nakagawa, Light-driven motion of liquids on a photoresponsive surface, *Science* **288**, 1624 (2000).
- [30] K. Nagai, Y. Sumino, H. Kitahata, and K. Yoshikawa, Mode selection in the spontaneous motion of an alcohol droplet, *Phys. Rev. E* **71**, 065301(R) (2005).
- [31] Y.-J. Chen, Y. Nagamine, and K. Yoshikawa, Self-propelled motion of a droplet induced by Marangoni-driven spreading, *Phys. Rev. E* **80**, 016303 (2009).
- [32] B. Reichert, J.-B. Le Cam, A. Saint-Jalmes, and G. Pucci, Self-propulsion of a volatile drop on the surface of an immiscible liquid bath, *Phys. Rev. Lett.* **127**, 144501 (2021).

- [33] S. Michelin, E. Lauga, and D. Bartolo, Spontaneous autophoretic motion of isotropic particles, *Phys. Fluids* **25**, 061701 (2013).
- [34] Z. Izri, M. N. Van Der Linden, S. Michelin, and O. Dauchot, Self-propulsion of pure water droplets by spontaneous Marangoni-stress-driven motion, *Phys. Rev. Lett.* **113**, 248302 (2014).
- [35] C. Jin, C. Krüger, and C. C. Maass, Chemotaxis and autochemotaxis of self-propelling droplet swimmers, *Proc. Natl. Acad. Sci. USA* **114**, 5089 (2017).
- [36] S. Michelin, Self-propulsion of chemically active droplets, *Annu. Rev. Fluid Mech.* **55**, 77 (2023).
- [37] C. C. Maass, C. Krüger, S. Herminghaus, and C. Bahr, Swimming droplets, *Annu. Rev. Condens. Matter Phys.* **7**, 171 (2016).
- [38] B. V. Hokmabad, R. Dey, M. Jalaal, D. Mohanty, M. Almukambetova, K. A. Baldwin, D. Lohse, and C. C. Maass, Emergence of bimodal motility in active droplets, *Phys. Rev. X* **11**, 011043 (2021).
- [39] Y. Tsoumpas, S. Dehaeck, A. Rednikov, and P. Colinet, Effect of Marangoni flows on the shape of thin sessile droplets evaporating into air, *Langmuir* **31**, 13334 (2015).
- [40] S. Shiri, S. Sinha, D. A. Baumgartner, and N. J. Ciria, Thermal Marangoni flow impacts the shape of single component volatile droplets on thin, completely wetting substrates, *Phys. Rev. Lett.* **127**, 024502 (2021).
- [41] See Supplemental Material at <http://link.aps.org/supplemental/10.1103/PhysRevFluids.9.L012001> for experimental recordings and related calculations.
- [42] H. Linke, B. J. Alemán, L. D. Melling, M. J. Taormina, M. Francis, C. C. Dow-Hygelund, V. Narayanan, R. P. Taylor, and A. Stout, Self-propelled Leidenfrost droplets, *Phys. Rev. Lett.* **96**, 154502 (2006).
- [43] D. Quéré, Leidenfrost dynamics, *Annu. Rev. Fluid Mech.* **45**, 197 (2013).
- [44] A. Bouillant, T. Mouterde, P. Bourrianne, A. Lagarde, C. Clanet, and D. Quéré, Leidenfrost wheels, *Nat. Phys.* **14**, 1188 (2018).
- [45] H. C. Berg, *Random Walks in Biology* (Princeton University Press, Princeton, 2018).
- [46] M. Polin, I. Tuval, K. Drescher, J. P. Gollub, and R. E. Goldstein, *Chlamydomonas* swims with two “gears” in a eukaryotic version of run-and-tumble locomotion, *Science* **325**, 487 (2009).
- [47] Y. Li, C. Diddens, P. Lv, H. Wijshoff, M. Versluis, and D. Lohse, Gravitational effect in evaporating binary microdroplets, *Phys. Rev. Lett.* **122**, 114501 (2019).
- [48] S. H. Davis, Thermocapillary instabilities, *Annu. Rev. Fluid Mech.* **19**, 403 (1987).
- [49] M. F. Schatz and G. P. Neitzel, Experiments on thermocapillary instabilities, *Annu. Rev. Fluid Mech.* **33**, 93 (2001).
- [50] K. Sefiane, J. R. Moffat, O. Matar, and R. Craster, Self-excited hydrothermal waves in evaporating sessile drops, *Appl. Phys. Lett.* **93**, 074103 (2008).
- [51] G. Karapetsas, O. K. Matar, P. Valluri, and K. Sefiane, Convective rolls and hydrothermal waves in evaporating sessile drops, *Langmuir* **28**, 11433 (2012).
- [52] W.-Y. Shi, K.-Y. Tang, J.-N. Ma, Y.-W. Jia, H.-M. Li, and L. Feng, Marangoni convection instability in a sessile droplet with low volatility on heated substrate, *Int. J. Therm. Sci.* **117**, 274 (2017).
- [53] P. Cerisier, S. Rahal, and N. Rivier, Topological correlations in Bénard-Marangoni convective structures, *Phys. Rev. E* **54**, 5086 (1996).
- [54] E. Koschmieder and S. Pahl, Surface-tension-driven Bénard convection in small containers, *J. Fluid Mech.* **215**, 571 (1990).
- [55] Q. Wang, R. Verzicco, D. Lohse, and O. Shishkina, Multiple states in turbulent large-aspect ratio thermal convection: What determines the number of convection rolls? *Phys. Rev. Lett.* **125**, 074501 (2020).